IET Renewable Power Generation

Research Article

IET Journals
The Institution of Engineering and Technology

Self-powered autonomous underwater vehicles: results from a gyroscopic energy scavenging prototype

ISSN 1752-1416
Received on 8th May 2015
Revised 18th December 2015
Accepted on 13th March 2016
E-First on 8th June 2016
doi: 10.1049/iet-rpg.2015.0210
www.ietdl.org

Nicholas C Townsend[1] ✉

[1]*Faculty of Engineering and the Environment, University of Southampton, Southampton SO16 7QF, UK*
✉ *E-mail: nick@soton.ac.uk*

Abstract: This study describes and presents preliminary experimental results from a novel prototype energy scavenging system installed in a model 2 m cylindrical autonomous underwater vehicle (AUV). The system, which is based on control moment gyroscope principles, utilises the gyroscopic response of a gimballed flywheel mounted within an AUV body to generate energy from the wave induced rotational motions of the vehicle. This method, using the reaction of a spinning wheel under an input torque to provide an output torque of greater magnitude, orthogonal to the input torque axis and the spin axis provides a means to harvest energy in-situ, without external appendages and additional hydrodynamic drag. The system promises to extend AUV mission durations indefinitely and reduce support vessel time currently required for periodical recharging and redeployment. A description of the system operation, design and experimental results from a series of regular wave tests conducted at zero speed in a towing tank are presented in this study. The results show that the system can harvest energy, with the greatest power generation around resonance, tailing off as the frequency increases and typically non-linear in nature. The system could potentially be applied to any rotationally excited platform e.g. autonomous surface vessels, buoys or boats

1 Introduction

Autonomous underwater vehicles (AUVs) have limited endurance capabilities [1]. Nearly all AUVs depend on stored energy for their operation [2]. Currently, the majority of AUVs use batteries as an energy supply for their operation [1, 3]. However, batteries have a finite life (stored energy), require periodical recharging (and redeployment) from a dedicated host platform or support vessel and represent a significant proportion of the total vehicle mass, typically around 20% [2]. A summary of various AUV sensors and AUV power requirements is given in Tables 1 and 2. With current AUV endurance, measured in hours or days [30], alternative power systems or in-situ charging strategies are required to extend missions.

With most of the oceans containing an average wind power density greater than 50 W/m^2 for more than 80% of the year (with a maximum of 1600 W/m^2) [31], an average solar energy power density at the surface of ~168 W/m^2 (~1270 W/m^2 at the limits of the atmosphere) [32] and the global oceans containing a wave energy density greater than 2 kW/m for 90% of the year (and wave energy densities greater than 20 kW/m in mid-latitudes) [33], the available ambient power is comparable to that required by an AUV. That is, energy scavenging systems, in particularly wave energy scavengers, promise to; enable AUV systems to be remotely and renewably recharged at sea, extend mission durations and capabilities, negate the necessity to carry sufficient energy reserves (size and weight) for entire mission(s), reduce costs by freeing support vessel time (a major cost component in AUV deployment) and provide flexibility in system deployment and recovery (time and/or location).

Solar powered AUVs and several solar assisted commercial ASVs systems, e.g. SAUV-II [34], Autonaut [35], WaveGlider [36] and C-Enduro [37], have been developed. While solar potentially offers unlimited mission durations, as found by the SAUV II it is limited to night-time missions and daylight recharging strategies and is susceptible to bio fouling [34]. A prototype thermal energy harvesting underwater vehicle, the SOLO-TREC, has also been developed, which uses a phase-change material (a waxy fluid) that melts and expands in warm water (at the surface) and solidifies in cooler (deeper) water to drive a hydraulic generator and provide power [38]. The SOLO-TREC is reported to provide over 7000 J

Table 1 Example AUV sensor power requirements

Sensor	Power, W
pressure sensor	0.1 (typ) [4]
digital compass	0.132 (typ), 0.014 (sleep) [5]
sound velocity sensor	0.25 (typ) [6]
echo sounder	0.25 (max) [7]
fluorometer	0.3 (typ) [8]
precision timing reference	0.3 (max) [9]
hydrophone	0.12–0.3 (typ) [10]
MEMS AHRS and GPS/INS	0.675–0.95 (typ) [11]
turbulence sensor	1 (typ) [12]
2D imaging sonar	3 (typ) [13]
CTD sensor	3.42 (incl. pump) [14]
digital camera	5 (typ) [15]
sidescan sonar	5 (typ exclude CPU) [16]
LBL acoustic positioning system	2.5–5.5 (transmit), 1.3 (max receive), 0.005–0.285 (listen mode), 0.0025 (standby) [17]
nitrate sensor	7.5 (max) [18]
Doppler velocity log	12 (max transmit), 2 (average transmit), 1.1 (typ) [19]
3D imaging sonar	15 (typ) [20]
underwater RF	16 (transmit), 5 (receive), 0.005 (sleep) [21]
current profiler	20–0.3 (transmit), 0.2–1.4 (typ) [22]
side scan sonar and sub bottom profiler	30 (max) [23]
navigation and control system	50 (max), 2 (active listening), 0.7 (sleep) [24]
multibeam swath bathymetry and sidescan	50 (max), 20 (standby) [25]
transponder	50 (max), 2 (active), 0.7 (sleep) [26]
underwater laser scanner	144 (typ) [27]
acoustic communications	300 (transmit), 1.8 (receive/standby), 0.08 (standby) [28]

Table 2 Example power consumption of various torpedo style battery powered AUVs [29]

Vehicle	Mass, kg	Length, m	Diameter, cm	Stored energy, kWh	Endurance, h	Power, W
Iver2-580-S	20.5	1.52	14.7	0.6	14	43
Folaga AUV	31.0	2.04	16.0	0.5	6	90
REMUS 100-S	38.5	1.60	19.0	1.0	10	100
REMUS 600	240.0	3.25	32.4	5.2	70	74
Bluefin 12D	260.0	4.32	32.0	7.5	30	250
Dorado class AUV	680.0	5.30	53.0	11.0	17.5	629
Bluefin 21	750.0	4.93	53.0	13.5	25	540
Abyss AUV	880.0	4.00	66.0	11.2	24	467
REMUS 6000	884.0	3.84	71.0	11.8	22	536
Eagle Ray AUV	940.0	4.60	69.0	29.4	30	979
Explorer-class MARUM SEAL AUV	1300.0	5.50	74.0	14.0	19	737
Echo Surveyor IV	1450.0	5.40	100.0	45.0	50	900

per dive, sufficient to power GPS, iridium and conductivity–temperature–depth (CTD) sensors [38]. In the past internal combustion engines have been used to power AUVs. However, these systems were found to be limited as additional power is needed to expel the exhaust gases at depths greater than 200 m [1]. Fuel cells have also been trialled, e.g. on the AUV URASHIMA [39] and IDEF Ifremer [40], however, these systems are expensive and complex [40]. The Royal Swedish Navy has used Stirling engines [1] and (Slocum) gliders have been developed using ocean temperature gradients and battery power to provide propulsion [41]. Various wind based concepts, e.g. C-enduro and the Submaran [42], are being developed. The C-enduro uses a deck mounted wind turbine to generate power and the Submaran uses a fixed wing (sail) for propulsion. Various sail based systems have also been developed for the Microtransat Challenge [43] – a fully autonomous sailing boat transatlantic race. Interestingly, no successful transit of the Atlantic within this competition has been made to date. Ideas of recharging AUV power supplies using wave-energy absorbers and sea current generators have also been proposed [44, 45], however, no practical demonstrations have been made. While wave propelled devices, e.g. the Autonaut and Wave Glider have been developed, these systems do not currently generate power. To date, no wave energy scavenging systems have been demonstrated.

This paper reports the results from the first demonstration of a gyroscopic wave-based energy scavenging system for an AUV. Currently gyroscopic wave energy converters (WECs) are gaining interest with several systems being developed in Japan [46–48], Italy [49–51] and Spain [52]. Unlike the systems being developed in Italy and Spain, with large, slow flywheels with limited precession and horizontal precession axis and the large (kW scale) WEC systems being developed in Japan, this study demonstrates:

- A small-scale system specifically for energy scavenging applications.
- A system with a vertical precession axis (whereby the rolling and pitching motions contribute to the energy harvested).
- A system with high flywheel *rpm* (thousands not hundreds).
- A system with unrestricted precession motion (where the gyroscopic precession can take any angle and the gyroscopic equations cannot necessarily be regarded as linear).

A detailed description of the principal of operation, system advantages and the prototype design is given in Section 2. The experimental setup and investigations are described in Section 3 and the results and discussion of results are presented in Section 4.

2 System description

2.1 Principal of operation

A schematic of the gyroscopic system is illustrated in Fig. 1. The system, which is based on control moment gyroscope (CMG) principles, utilises the gyroscopic response of a gimballed flywheel mounted within an AUV body to generate energy from the wave induced rotational motions of the vehicle.

The system equations of motion can be described by the Newton–Euler equations. Defining $\underline{\omega}_f$ and $\underline{I}_f$ as the flywheel angular velocities and mass moment of inertias of the flywheel, with respect to (X_f, Y_f, Z_f), the angular momentum of the flywheel can be expressed as

$$\underline{H}_f = \underline{I}_f \underline{\omega}_f \tag{1}$$

In the (AUV) body-fixed axis (X_b, Y_b, Z_b) this can be expressed as

$$\underline{H}_{b*} = \underline{\boldsymbol{A}}_f^b \underline{H}_f \tag{2}$$

where $\underline{\boldsymbol{A}}_f^b$ represents the rotation matrix describing the transformation of the momentum component from (X_f, Y_f, Z_f) to (X_b, Y_b, Z_b). Including the AUV motion, the moments acting around each axis in the AUV body-fixed coordinate frame (X_b, Y_b, Z_b) can then be expressed as

$$\dot{\underline{H}}_b = \dot{\underline{H}}_{b*} + \underline{\Omega}^{\times} \underline{H}_{b*} \tag{3}$$

where $\dot{\underline{H}}_b$ represents the moments acting around each axis in the (AUV) body-fixed coordinate frame, $\underline{\Omega}^{\times}$ represents the skew-symmetric form (equivalent to the cross product operation) of the (AUV) body motions experienced by the flywheel. $\underline{H}_{b*}$ represents angular momentum of the flywheel in the AUV body-fixed axis system (X_b, Y_b, Z_b). Assuming, as illustrated in Fig. 1, the flywheel is restricted about the x-axis (X_f), precesses about the z-axis (Z_f) and has an angular velocity, $\dot{\psi}$, about the y-axis (Y_f) and the flywheel and AUV centres of mass lie at the origin of the body-frames of reference and the body-frames of reference coincide with the principal axes of inertia of the bodies. As shown in [53], (3) can be expanded yielding the torque about the precession axis ($Z_f = Z_b$)

$$\tau_p = I_{zz}\ddot{\beta} - I_{yy}\dot{\psi}\dot{\phi}\sin\beta + I_{yy}\dot{\psi}\dot{\theta}\cos\beta \tag{4}$$

Here I_{xx}, I_{yy}, I_{zz} represent the mass moment of inertia about the flywheel fixed axis, spin axis and precession axis, respectively. $\dot{\psi}$ represents the flywheel spin rate and $\dot{\theta}, \dot{\phi}$ represent the roll and pitch angular velocities of the AUV body, respectively. τ_p, β represent the torque about the precession axis and the precession angle, respectively. Equation (3) shows that with AUV roll and pitch motions ($\dot{\theta}, \dot{\phi}$) a gyroscopic precession ($\dot{\beta}$) and a precession torque (τ_p) is experienced. That is, with precession motion and precession torque, the precession axis can be used to drive a generator and produce power.

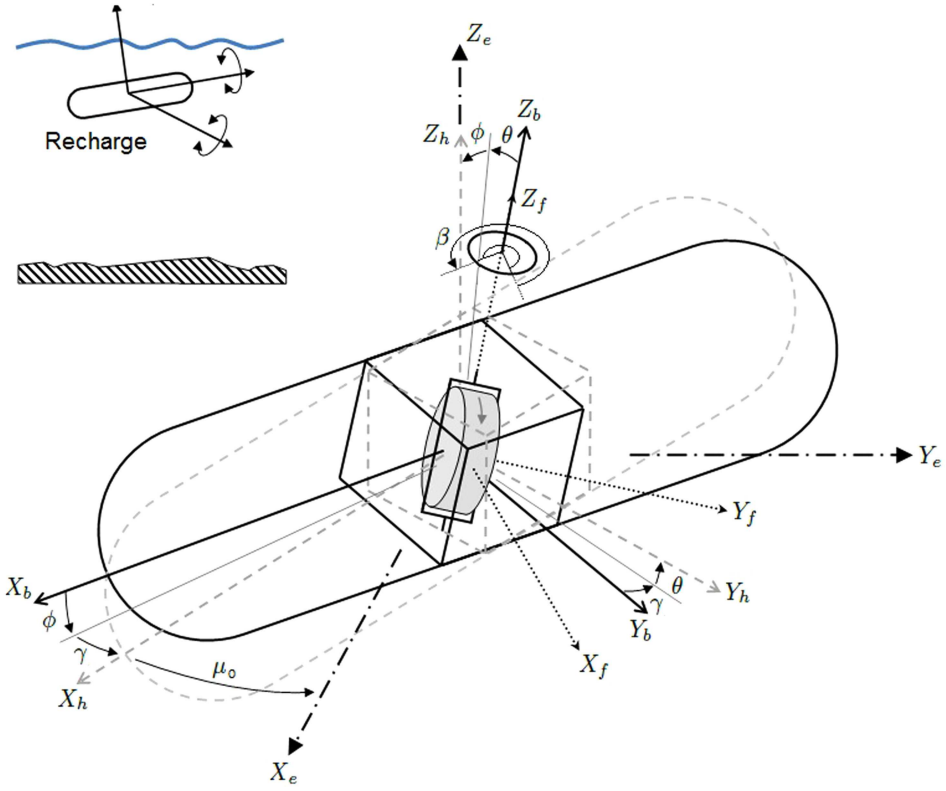

Fig. 1 *System schematic and coordinate frame definitions [(X_e, Y_e, Z_e) represents an Earth fixed inertial axis system, (X_h, Y_h, Z_h) represents the hydrodynamic or equilibrium axis system that moves with the average motion of the AUV, but is not fixed to the AUV, (X_b, Y_b, Z_b) represents the body (AUV)-fixed axis system, and (X_f, Y_f, Z_f) represents the flywheel axis system. This axis precesses, but does not spin with the flywheel]*

2.2 System advantages (and disadvantages)

The system utilises the reaction of a spinning wheel under an input torque (AUV motion) to provide an output torque of greater magnitude, orthogonal to the input torque axis and the spin axis to drive a generator. This provides a means to harvest energy in-situ with no external appendages, avoiding any additional hydrodynamic drag. Furthermore, with no direct exposure to the marine environment the system is not susceptible to environmental performance degradations, i.e. bio fouling and would not be limited to daylight recharging and night time missions. Potentially the system could be applied to any rotational excited platform(s), e.g. ASVs, boats, buoys and WECs.

In practice as the effect of surface waves and swell diminishes with depth [54], similar to solar-based AUVs (e.g. SAUV II), the AUV system would need to surface to recharge, as depicted in Fig. 1 – admittedly exposing the AUV to the potentially hazardous wave environment. However, as waves are a concentrated form of solar energy (formed by winds passing over bodies of water created by the differential heating of air masses by the sun on the earth's atmosphere) with a reported spatial concentration of time-averaged power flow of typically 0.1–0.3 kW/m^2 (solar) to 0.5 kW/m^2 (wind) to 2–3 kW/m^2 (wave) [55], greater energy capture is anticipated compared to solar and wind strategies.

2.3 Prototype design

The prototype design is illustrated in Figs. 2*a*–*c*. Based on the majority of AUV systems, a torpedo style AUV, with a cylindrical body design was selected. The body diameter ($\simeq$ 30 cm) was approximately based on the REMUS 600 AUV, see Table 2. To minimise the swept volume and mass, the flywheel was designed to precess about the central axis of the flywheel, with the flywheel thickness comparable to the flywheel diameter, with an I-shaped cross section. The gyroscopic system was designed to allow full, unrestricted 360° precession motion. This was achieved by using a slip ring mounted on the precession axis to provide power to the spin motor. To convert the mechanical power to electrical power a DC generator (motor) was employed. A discussion of the generator efficiency is given in Section 4.5. A summary of the AUV, gyroscopic unit and generator particulars are presented in Table 3.

3 Experimental setup and investigations

A series of regular wave tests over a range of frequencies (0.5–1.4 Hz) and wave amplitudes (0.1 and 0.05 m) were conducted in a towing tank with the gyroscopic system operating (within the AUV) at several spin rates (1000, 5000 and 9000 rpm) and with the system disabled. The prototype was tested following a conventional sea keeping methodology, with the AUV attached to the tow post of the towing tank carriage, constraining the AUV in yaw, roll, surge and sway. For comparison, a series of slack moored tests were also conducted. The experimental setups are illustrated in Fig. 2. The generated data was logged at 100 Hz (using a National Instruments compactRIO). The generated power was calculated by measuring the voltage (V_r) across a resistor (R_r) connected to the terminals of the generator, i.e. $P = V_r^2/R_r$. The generator particulars are summarised in Table 3.

4 Results and discussion

The following results are presented in this section:

- 3: The equivalent harvested energy (Wh) over a range of frequencies and spin rates, per hour.
- 4: The generated power (peak and rms) over a range of frequencies, spin rates, wave heights and constraints.

Table 3 System particulars

AUV system particulars	Value
overall length (L_b), m	2
diameter, m	0.2929
assembled AUV prototype mass, kg	110.3
trim angle, deg.	11.8

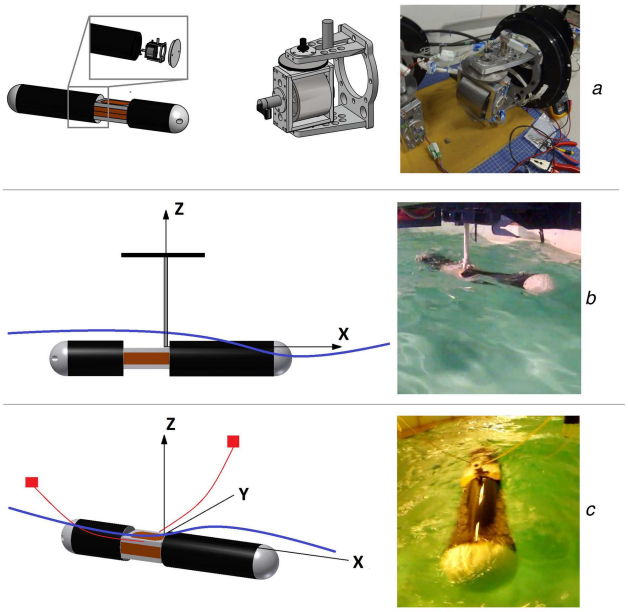

Fig. 2 *Prototype system and experimental setups*
(a) CAD assembly and manufactured gyroscopic unit, ***(b)*** Experimental tow-post arrangement, ***(c)*** Experimental slack moored arrangement

- 5: The non-dimensional pitch response ($\phi_a/k\zeta_a$) of the AUV over a range of frequencies. That is, the AUV motion response in waves without the gyroscopic system operating.
- 6: Example gyroscopic precession angle variation over time.

These results are based on ten wave encounters. Example time and frequency domain responses are presented in Figs. 7*a–c* and 8*a–c* and flywheel acceleration and deceleration profiles (on start-up and shutdown) are also presented in Fig. 9.

Fig. 3 shows the harvested energy per hour, calculated by integrating the power profiles over ten wave encounters and extrapolating to a one-hour period. The results show that the harvested energy is greatest around resonance, tailing off as the frequency increases.

To provide a representative comparison, as the wave amplitudes were found to vary slightly between tests, the generated power (over the ten wave encounters) were normalised with respect to the (maximum) wave amplitude, see Fig. 4. The results show that the power generated is greatest around resonance ($\simeq 0.7$ Hz) and rapidly reduces at higher frequencies (e.g. above 1 Hz). Furthermore, the results show that the maximum instantaneous power compared to the rms power is large (up to six times), indicating that the generated power is not sinusoidal.

As shown in Figs. 7 and 8, the generated power 'pulses', as the flywheel precesses and drives the generator. Interestingly, the pulses can vary in frequency and magnitude over time and are rarely proportional to the (regular) wave frequency. That is, the generated power is typically non-linear. Although this finding is not unexpected (see [56]), the non-linear responses were found to be readily achievable, particularly the case of continuous precession rotation, see Fig. 6*a*. As a continuous precession motion can be achieved, a continuous power output is possible with the system. With a 1 degree of freedom excitation it is known that when the flywheels orientate themselves in line with the forcing excitation, no gyroscopic precession can occur and no energy can be harvested [56]. In practise, it is anticipated that any slight additional axial excitation will 'kick' the system out of these dead zones and this may account for the irregular power output. Furthermore, these results indicate that an optimised restoring term and/or control of the gyroscopic precession (position and rate) could further increase the energy harvested and widen the operating range.

4.1 Spin rate

With low spin rates, e.g. 1000 rpm, the gyroscopic torque is small and no significant power is generated. Generally increasing the spin rates, greater powers (peak and *rms*) were observed. However, the difference between 5000 and 9000 rpm does not appear to represent a significant step change in the generated power. At these spin rates, the system response can become non-linear and it is expected that the flywheel orientation is not always optimally aligned with the wave induced excitation, reducing the energy capture (see Fig. 6*b*), and that there is an optimal spin rate for a given condition and system setup.

4.2 AUV motion

Fig. 5 shows the non-dimensional pitch response, a measure of the pitch amplitude relative to the wave slope, of the AUV prototype. This was calculated from the pitch angular velocity amplitude, i.e. $\dot{\phi}_a = \phi_a\omega$, $k = \omega^2/g$. The pitch angular velocity, $\dot{\phi}$, was measured with a xSENS MTi-100 inertial measurement unit. The response shows a characteristic resonance response, around 0.7 Hz, with the motion amplitude decreasing with increasing frequency. For the investigated conditions, the AUV motion responses are relatively small, with the largest investigated case ($\zeta_a \simeq 10$ cm) equating to a peak pitch amplitude response of approximately 7.5°. That is, the test conditions represent a relatively benign sea state and AUV response. As shown in Fig. 4*b*, greater power can be generated in larger waves. Therefore in a real seaway, where larger waves and responses are expected, it is anticipated that greater power can be generated from the system than presented.

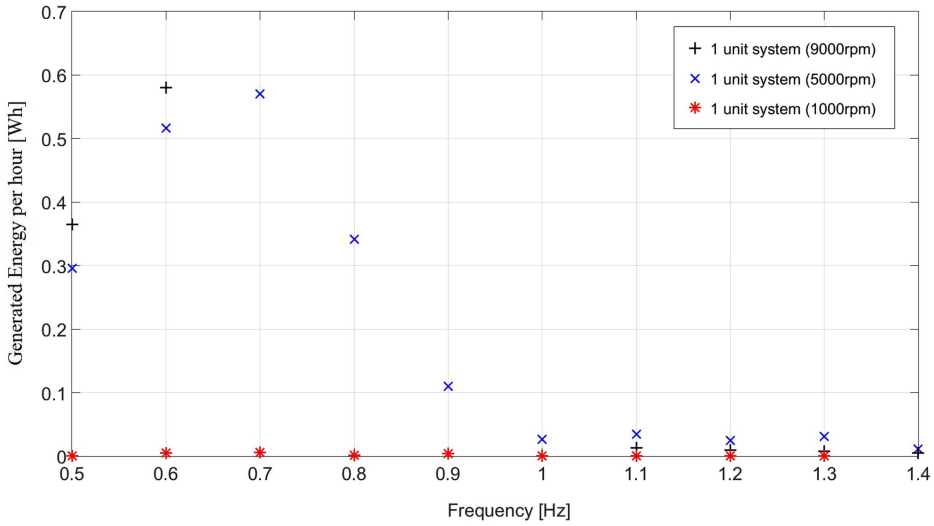

Fig. 3 *Equivalent harvested energy (Wh per hour) over a range of frequencies, spin rates ($\zeta_a \simeq 10$ cm)*

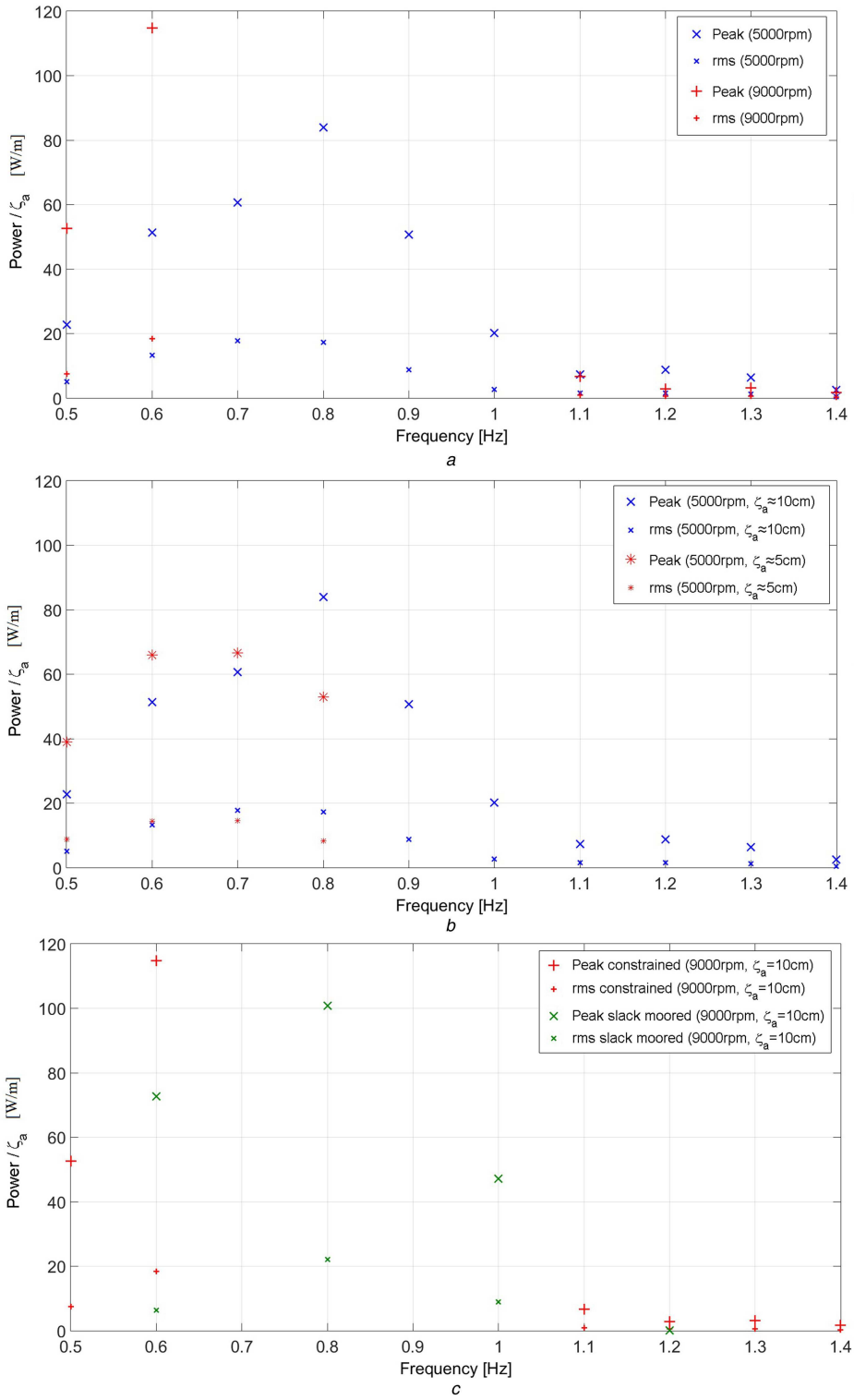

Fig. 4 *Peak and rms generated power*

(a) Over a range of frequencies and spin rates ($\zeta_a \simeq 10$ cm, 5000 rpm and 9000 rpm), ***(b)*** Over a range of frequencies and wave heights ($\zeta_a \simeq 5$ cm and $\simeq 10$ cm, 5000 rpm), ***(c)*** With tow-post and slack moored constraints ($\zeta_a \simeq 10$ cm, 9000 rpm

4.3 Experimental setup

The prototype was tested following a conventional sea keeping methodology, with the AUV attached to the tow post of the towing tank carriage, constraining the AUV in yaw, roll, surge and sway. Varying the experimental constraint, in Fig. 4*c* the results were found to be similar in magnitude for a slack moored and tow post constrained setup. The results provide some confidence that the constraint does not significantly influence the system. However, the constraint is believed to influence the system response and a more detailed study is needed to identify the effect(s).

4.4 Energy balance

Fig. 9 shows an example, acceleration and deceleration profiles for the prototype. As the system requires power to initially accelerate and then maintain the flywheel spin rate, overcoming friction, an estimate of the input power to accelerate the flywheel and the power to overcome friction and maintain the flywheel *rpm* was made.

Assuming a constant energy loss, the power loss due to friction (to maintain the flywheel *rpm*) was estimated as

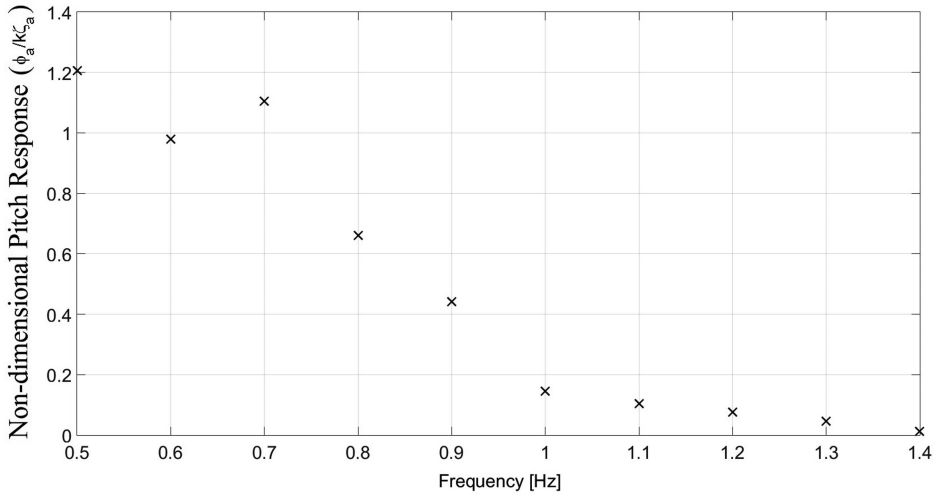

Fig. 5 *Non-dimensional pitch response ($\phi_a/k\zeta_a$) of the AUV in regular waves (system off)*

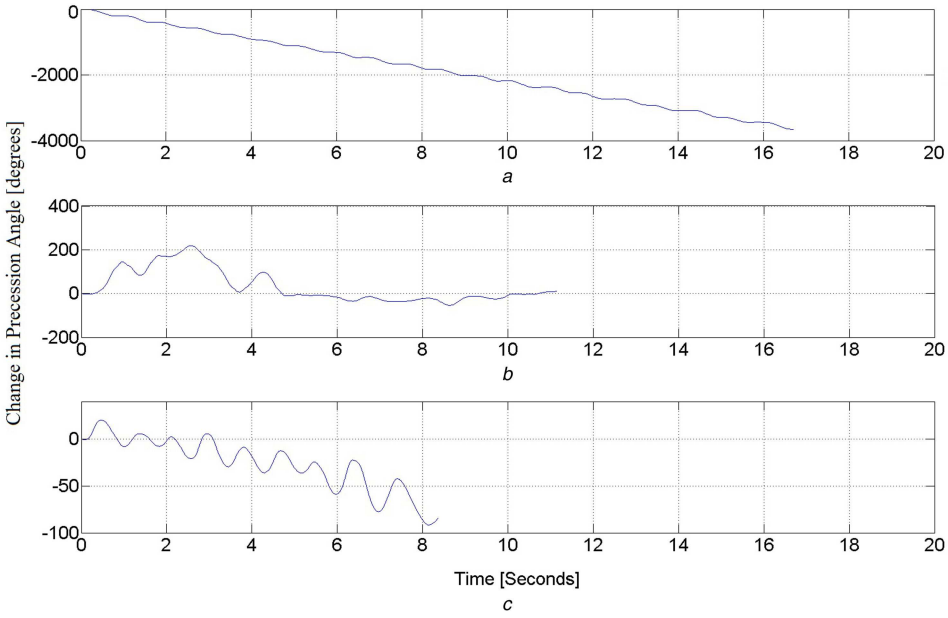

Fig. 6 *Change in precession angle over time $\zeta_a \simeq 10$ cm, 5000 rpm, 10 wave encounters*
(a) 0.6 Hz, ***(b)*** 0.9 Hz, ***(c)*** 1.2 Hz

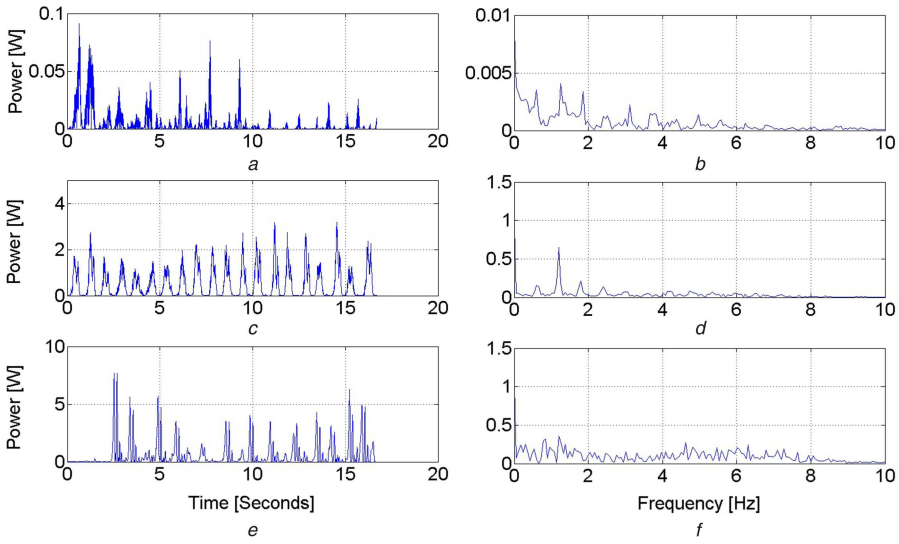

Fig. 7 *Example time histories and fast Fourier transforms (FFT) of generated power $\zeta_a \simeq 10$ cm, 0.6 Hz*
(a) 1000 rpm time history, ***(b)*** 1000 rpm FFT, ***(c)*** 5000 rpm time history, ***(d)*** 5000 rpm FFT, ***(e)*** 9000 rpm time history, ***(f)*** 9000 rpm FFT

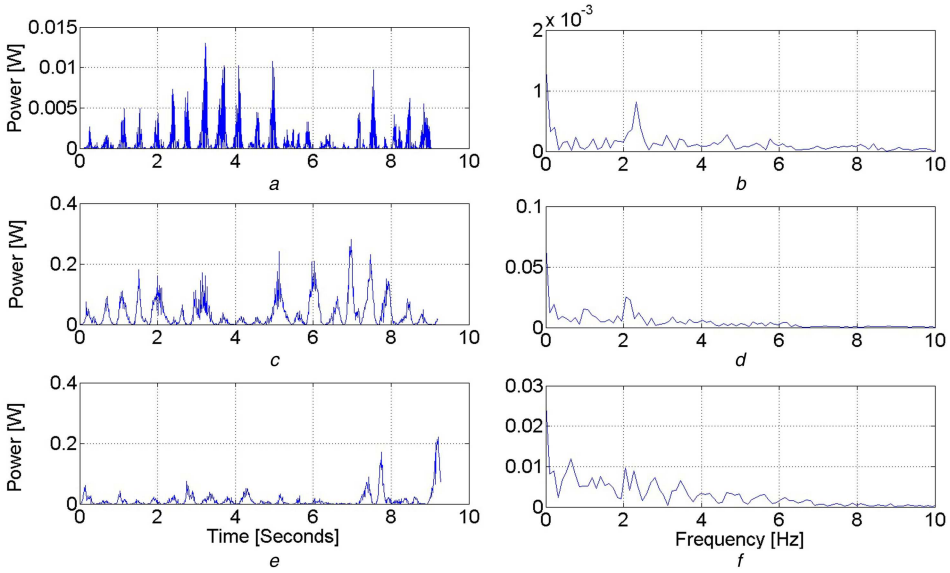

Fig. 8 *Example time histories and FFT of generated power $\zeta_a \simeq 10$ cm, 1.1 Hz*
(a) 1000 rpm time history, ***(b)*** 1000 rpm FFT, ***(c)*** 5000 rpm time history, ***(d)*** 5000 rpm FFT, ***(e)*** 9000 rpm time history, ***(f)*** 9000 rpm FFT

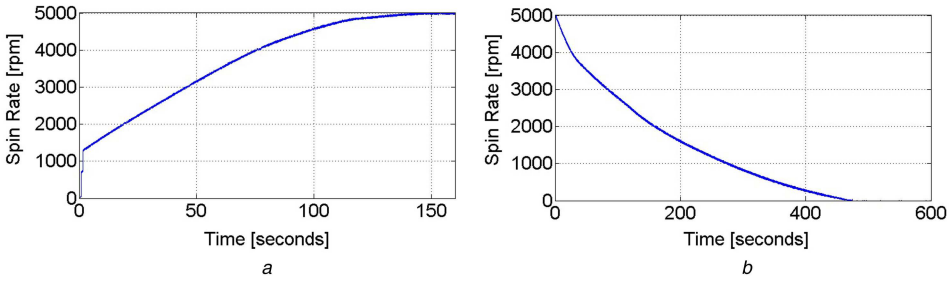

Fig. 9 *Flywheel acceleration and deceleration profiles*
(a) Flywheel spun up to 5000 rpm, ***(b)*** Flywheel spun down from 5000 rpm

$$P = \frac{1}{2} I_{yy} \omega_{\mathrm{f}}^2 / t \tag{5}$$

where $(1/2) I_{yy} \omega_{\mathrm{f}}^2$ represents the stored kinetic energy in the flywheel. As the prototype system takes ~470 s for the flywheel to slow from 5000 rpm to rest, see Fig. 9*b*, the power loss due to friction was estimated as

$$P = (0.5 \times 0.00482 \times (5000 \times 2\pi/60)^2)/470 \simeq 1.4\,\mathrm{W}$$

That is, a continuous power input of 1.4 W (estimate) was required to maintain the flywheel at its operating spin rate. Similarly, the input power to accelerate the flywheel was calculated, see Fig. 9*a*, yielding approximately a 4 W power demand for a 160 s start up time, assuming no losses. Considering the supplied current was limited to 4 A and 24 V ($\simeq$ 100 W), or considering the motor rating (40 W), the efficiency of start-up of the prototype system is estimated at between 4 and 10%.

4.5 Generator efficiency

Expressing the generator overall efficiency as the ratio of electrical power output, P_{e}, to the mechanical power input, P_{m}:

$$\eta_{\mathrm{pto}} = \frac{P_{\mathrm{e}}}{P_{\mathrm{m}}} \tag{6}$$

and estimating the electrical power and mechanical power delivered to the generator as

$$P_{\mathrm{e}} = \frac{V^2}{R} \tag{7}$$

and

$$P_{\mathrm{m}} = \frac{\tau_{\mathrm{p}}}{g} g\dot{\beta} \tag{8}$$

respectively, where τ_{p}/g and $g\dot{\beta}$ represents the torque and angular velocity at the generator shaft, respectively, and g represents the gearing between the gyroscopic precession axis and the generator shaft. In addition, estimating the magnitude of the gyroscopic torque τ_{p}, as

$$\tau_{\mathrm{p}} \simeq I_{yy} \dot{\psi} \dot{\phi} \tag{9}$$

Then, the estimated mechanical power delivered to the generator shaft (using the rms and maximum measured values for V, $\dot{\phi}$ and $\dot{\beta}$), as shown in Figs. 10*a* and *b* (for a spin rate of 5000 rpm), is between 0.05–4 W *rms* and 0.4–18 W peak. In comparison the electrical power ranged from 0.02–0.8 W rms to 0.14–3.2 W peak. That is, the estimated efficiency of the prototype generator is estimated to be $\simeq$ 30% (ranging between 14 and 50%), as shown in Fig. 10.

In the tested conditions, the prototype system generated power up to 0.8 rms (3.2 peak) W with $\dot{\psi} = 5000$ rpm and up to 1.24 rms (8 peak) W with $\dot{\psi} = 9000$ rpm (see Fig. 10). This shows that the system can harvest energy, however, given the estimated power loss due to friction in the tested conditions a net gain may not have been achieved. Given that the investigated conditions and responses were relatively small and that the estimated mechanical energy delivered to the generator shaft is typically greater than the friction loss (see Fig. 10). Then a net gain appears readily feasible with operation in larger waves and/or improved generator efficiency [e.g. if $\eta_{\mathrm{pto}} = 100\%$ (instead of $\simeq$ 30%) then the system could be expected to generate up to 2.67 rms (10.67 peak) W with

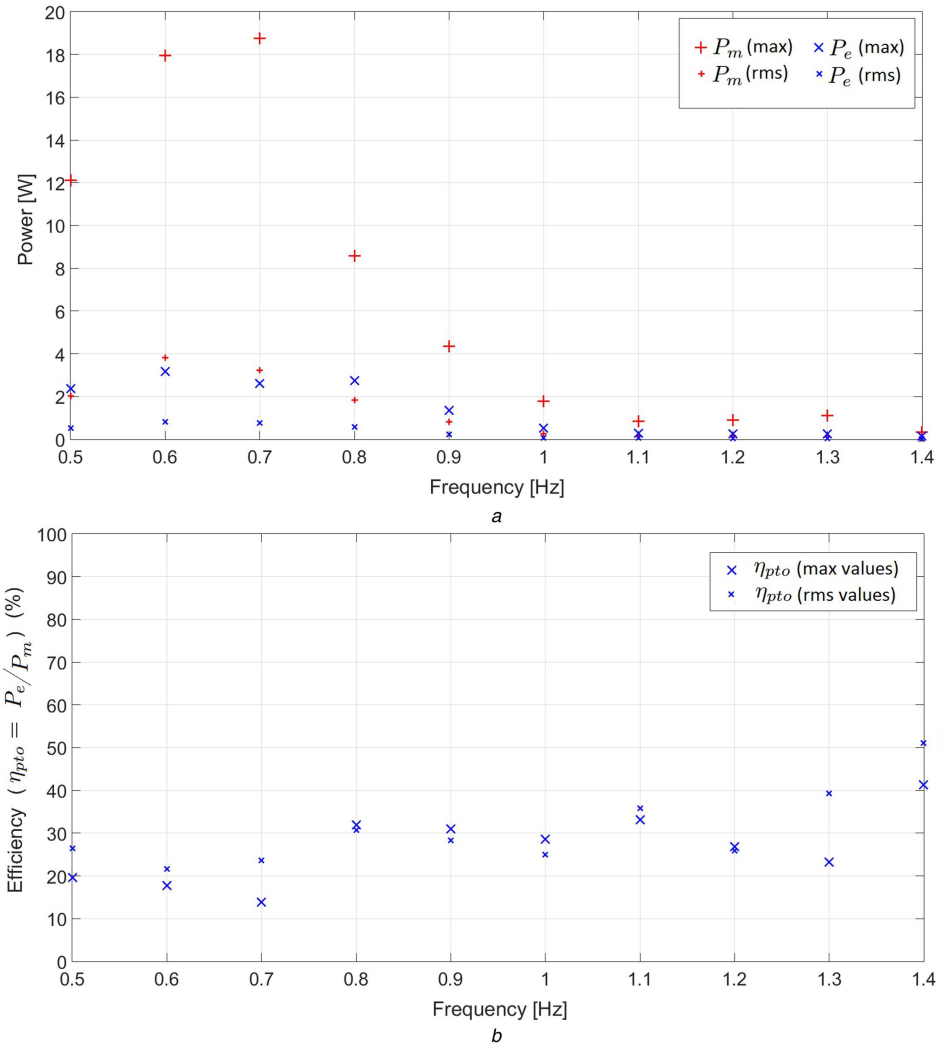

Fig. 10 *Generator efficiency*
(a) Mechanical power (P_m) and electrical power (P_e), ***(b)*** Percentage efficiency

$\dot{\psi} = 5000$ rpm and up to 4.12 rms (26.67 peak) W with $\dot{\psi} = 9000$ rpm]. This could be achieved by controlling the torque and rpm delivered to the generator, for example through the use of a controlled, variable gearing between the precession axis and generator shaft. Compared to other energy scavenging systems, Table 4, and AUV powering requirements, Tables 1 and 2, the results are very encouraging.

5 Conclusions

This paper describes a novel prototype energy scavenging system for a torpedo style AUV. The system, based on CMG principles, provides a means to harvest (wave) energy in-situ, internally, without external appendages. A description of the system operation, design and experimental results from a series of regular wave tests conducted at zero speed in a towing tank are presented. The results show that the system can harvest energy, although in the tested conditions a net energy gain was not achieved. In the tested conditions ($\zeta_a \simeq 10$ cm), equating to a maximum (AUV) pitch response of 7.5°, the prototype system harvested the equivalent of between 0.05 and 0.6 Wh per hour, with a maximum recorded peak power of 8 W. The generated power was found to be the greatest around resonance, tailing off as the wave frequency increased. Typically, greater spin rates and wave amplitudes yielded greater power with the response becoming increasingly non-linear.

The experimental results show that the system has the potential to provide additional hotel load or power specific systems on an AUV or similarly rotationally excited platform, e.g. ASVs, buoys or boats.

Table 4 Comparison to other energy scavenging systems

Prototype gyroscopic system	Power	Notes
power (actual)	up to 0.8–1.2 W (rms) 3.2–8 W (peak)	$\dot{\psi} = 5000 - -9000$ rpm (note: $\zeta_a <$ 10 cm) (ignoring frictional losses)
power per wave amplitude	up to 20 W/m (rms) 80–115 W/m (peak)	$\dot{\psi} = 5000 - -9000$ rpm, $\zeta_a \simeq 10$ cm (ignoring frictional losses)
power (maximum – if $\eta_{pto} = 100\%$)	up to 2.6–4.1 W (rms) 10.7–26.7 W (peak)	$\dot{\psi} = 5000 - -9000$ rpm (note: $\zeta_a <$ 10 cm) (ignoring frictional losses)

6 Acknowledgment

This research was funded by the Defence Science and Technology Laboratory (DSTL) through the Centre for Defence Enterprise (CDE).

7 References

[1] Reader, G., Potter, J., Hawley, J.: 'The evolution of AUV power systems'. OCEANS '02 MTS/IEEE, 2002, vol. **1**, pp. 191–198
[2] Griffiths, G., Jamieson, J., Mitchell, S., *et al.*: 'Energy storage for long endurance AUVs'. Proc. of Advances in Technology for Underwater Vehicles, London, UK, 2004, pp. 8–16

[3] Griffiths, G., Reece, D., Blackmore, P., *et al.*: 'Modeling hybrid energy systems for use in AUVs'. Proc. 14th Unmanned Untethered Submersible Technology (UUST), 2005

[4] Paroscientific series 9000 pressure instrument. Available at: http://www.auvac.org/sensors/view/23?fromsearch=1

[5] Dc-4e digital compass. Available at: http://www.spartonnavex.com/product/dc-4e/

[6] Valeport ultra sv (sound velocity sensor) specification sheet. Available at: http://www.valeport.co.uk/Portals/0/Docs/Datasheets/Valeport_ultraSV_v2a.pdf

[7] Imagenex model 853 scientific echo sounder with data logger specification sheet. Available at: http://www.auvac.org/uploads/manufacturer_spec_sheet_pdf_sonar/Imagenex%20853_ES_with_Data_Logger_Specs_rev4.pdf

[8] Cyclops-6k submersible sensors specification sheet. Available at: http://www.turnerdesigns.com/products/submersible-fluorometer/cyclops-6k-6000-meter-submersible-fluorescence-and-turbidity-sensors

[9] L-3 nautronix, high precision timing reference (hptr) performance specification sheet. Available at: http://www.auvac.org/uploads/manufacturer_spec_sheet_pdf_nav/HPTRRev_2.1.pdf

[10] Sparton phod-1 hydrophone specification. Available at: http://www.spartonnavex.com/product/phod-1-hydrophone/

[11] xsens mti 100-series brochure. Available at: https://www.xsens.com/wp-content/uploads/2013/12/MTi-100-series1.pdf

[12] Microrider-1000 modular, self-contained turbulence profiler data sheet. Available at: http://www.rocklandscientific.com/LinkClick.aspx?fileticket=2QpE2AQoUco%3d&tabid=133

[13] 2d imaging sonar data sheet. Available at: http://www.auvac.org/uploads/manufacturer_spec_sheet_pdf_sonar/Data_Sheet_P900-90_v2.pdf

[14] Sbe 49 fastcat ctd sensor specification sheet. Available at: http://www.seabird.com/sbe49-fastcat-ctd

[15] High resolution ccd camera data sheet. Available at: http://www.alliedvisiontec.com/us/products/cameras/gigabit-ethernet/prosilica-ge/ge1900.html

[16] Sea scan pc auv specification sheet. Available at: http://www.marinesonic.us/products/SSPCAUV/sspc-auv-documents/Sea%20Scan%20PC%20AUV%20Specifications.pdf

[17] Lbl positioning and communication systems: product information guide. Available at: http://www.auvac.org/uploads/manufacturer_spec_sheet_pdf_nav/EvoLogics_S2CR_LBL_a4.pdf

[18] Suna v2 uv nitrate sensor specification sheet. Available: http://www.satlantic.com/suna?qt-product_tabs=1#qt-product_tabs

[19] Explorer pa Doppler velocity log (dvl) brochure. Available at: http://www.auvac.org/uploads/manufacturer_spec_sheet_pdf_nav/explorer_ds_lr.pdf

[20] Mb1350-45, 3d ultra-high resolution microbathymetry brochure. Available at: http://www.auvac.org/uploads/manufacturer_spec_sheet_pdf_sonar/MB1350-45v2.pdf

[21] Wfs technologies: Seatooth s200 underwater rf, product information. Available at: http://www.auvac.org/comms/view/6?from_search=1

[22] Aquadopp current meter product brochure. Available at: http://www.nortek-as.com/lib/brochures/aquadopp-current-meter

[23] 2200-s, survey quality sonars for small auvs, product information. Available at: http://www.auvac.org/uploads/manufacturer_spec_sheet_pdf_sonar/EdgeTech%202200-s_brochure.pdf

[24] Avtrak 6 (omni-directional version) data sheet. Available at: http://www.auvac.org/uploads/manufacturer_spec_sheet_pdf_nav/Sonardyne_8220_av6.pdf

[25] Kongsberg geoacoustics wide swath bathymetry for auvs, product information. Available at: http://www.auvac.org/uploads/manufacturer_spec_sheet_pdf_sonar/GeoSwath-ROV-AUV.pdf

[26] Avtrak 2 (omni-directional version) data sheet. Available at: http://www.auvac.org/uploads/manufacturer_spec_sheet_pdf_sonar/sonardyne_8065_avtrak2.pdf

[27] Uls-500 underwater laser scanner for long range scans, product brochure. Available at: https://www.oceanologyinternational.com/__novadocuments/18127?v=634886964440300000

[28] L-3 oceania gpm300 acoustic modem, data sheet. Available at: http://www2.l-3com.com/oceania//pdfs/datasheets/GPM%20300%20Acoustic%20Modem%20Spec%20Sheet%20Rev%201%206.pdf

[29] Wynn, R., Linley, E., Hunt, J.: 'Global inventory of auv and glider technology available for routine marine surveying'. Available at: http://www.nerc.ac.uk/innovation/activities/infrastructure/offshore/catalogue-of-auvs.pdf

[30] Button, R., Kamp, J., Curtin, T., *et al.*: '*A survey of missions for unmanned undersea vehicles*' (National Defense Research Institute, The RAND Corporation, 2009)

[31] wei Zheng, C., Pan, J.: 'Assessment of the global ocean wind energy resource', *Renew. Sustain. Energy Rev.*, 2014, **33**, (0), pp. 382–391. Available at: http://www.sciencedirect.com/science/article/pii/S1364032114000860

[32] Hermann, W.A.: 'Quantifying global exergy resources', *Energy*, 2006, **31**, (12), pp. 1685–1702. Available at: http://www.sciencedirect.com/science/article/pii/S0360544205001805

[33] Zheng, C., Shao, L., Shi, W., *et al.*: 'An assessment of global ocean wave energy resources over the last 45 a', *Acta Oceanol. Sinica*, 2014, **33**, (1), pp. 92–101. Available at: http://dx.doi.org/10.1007/s13131-014-0418-5

[34] Crimmins, D., Patty, C., Beliard, M., *et al.*: 'Long-endurance test results of the solar-powered AUV system'. OCEANS '06, 2006, pp. 1–5

[35] Autonaut specifications. Available at: http://www.autonautusv.com/specifications

[36] Liquid robotics product specifications. wave glider sv2. Available at: http://www.ofeg.org/np4/file/66/2013_Liquid_Robotics_Wave_Gliders_SV2.pdf

[37] Asv c-enduro. long endurance marine unmanned surface vehicle (lemusv) product brochure. Available at: http://www.asvglobal.com/files/datasheets/c-enduro-datasheet.pdf

[38] Yi, C.: 'Thermal recharging battery for underwater instrumentations'. Ocean Bottom Seismograph (OBS) Workshop, Redondo Beach, California, 2013

[39] Hyakudome, T., Aoki, T., Murashima, T., *et al.*: 'Key technologies for AUV 'URASHIMA''. OCEANS '02 MTS/IEEE, 2002, vol. **1**, pp. 162–166

[40] Mendez, A., Leo, T., Herreros, M.: 'Current state of technology of fuel cell power systems for autonomous underwater vehicles', *Energies*, 2014, **7**, (7), pp. 4676–4693

[41] Davis, R., Eriksen, C., Jones, P.: '*Autonomous buoyancy-driven underwater gliders*', in Griffiths, G. [ed.], *The technology and applications of autonomous underwater vehicles*. (Taylor and Francis, Abingdon, 2002), pp. 37–58

[42] Ocean aero. unmanned underwater/surface vessel uusv product brochure. Available at: http://www.oceanaero.us/OAHandout9.pdf

[43] The microtransat challenge. Available at: http://www.microtransat.org/

[44] Camilli, R., Bowen, A., Farr, N.: 'Bright Blue: advanced technologies for marine environmental monitoring and offshore energy'. OCEANS '10, 2010

[45] Hagerman, G.: 'Wave energy systems for recharging AUV energy supplies'. Proc. of the Symp. on Autonomous Underwater Vehicle Technology, 2002, pp. 75–84

[46] Kanki, H.: 'Gyro wave activated power generator and a wave suppressor using the power generation'. Patent US 7,003,947 B2, 2006

[47] Kanki, H., Arii, S., Furusawa, T., *et al.*: 'Development of advanced wave power generation system by applying gyroscopic moment'. Proc. of the 8th European Wave and Tidal Energy Conf. (EWTEC), Uppsala, Sweden, 2009, pp. 280–283

[48] Kanki, H., Morimoto, T., Kawanishi, M., *et al.*: 'Study on dynamics of floating wave-power generating system using gyro moment', *Jpn Soc. Mech. Eng.*, 2005, **80**, pp. 6.57–6.58

[49] Bracco, G., Giorcelli, E., Marignetti, F., *et al.*: 'ISWEC: Application of linear tubular generators'. IEEE Int. Symp. on Industrial Electronics, 2010, pp. 2426–2430

[50] Bracco, G., Giorcelli, E., Mattiazzo, G.: 'ISWEC: a gyroscopic mechanism for wave power exploitation', *Mech. Mach. Theory*, 2011, **46**, (10), pp. 1411–1424

[51] Bracco, G., Giorcelli, E., Mattiazzo, G., *et al.*: 'ISWEC: design of a prototype model with gyroscope'. Int. Conf. on Clean Electrical Power, 2009, pp. 57–63

[52] Salcedo, F., Ruiz-Minguela, P., Rodriguez, R., *et al.*: 'OCEANTEC: sea trials of a quarter scale prototype'. Proc. of 8th European Wave Tidal Energy Conf. (EWTEC), Uppsala, Sweden, 2009, pp. 460–465

[53] Townsend, N., Shenoi, R.: 'A gyroscopic wave energy recovery system for marine vessels', *IEEE J. Oceanic Eng.*, 2012, **37**, (2), pp. 271–280

[54] Levine, E., Goodman, L., Lubke, C.: 'AUV-based swell characterization'. IEEE/OES Autonomous Underwater Vehicles, 2008, pp. 1–6

[55] Falnes, J.: 'A review of wave-energy extraction', *Marine Struct.*, 2007, **20**, (4), pp. 185–201

[56] Townsend, N., Shenoi, R.: 'Modelling and analysis of a single gimbal gyroscopic energy harvester', *Nonlinear Dyn.*, 2013, **72**, (1), pp. 285–300

[57] Solar-powered auv: Sauvii white paper. Available at: http://www.falmouth.com/images/SAUVwhitePaper.pdf

[58] (2013, March) Practical boat owner. We got the power! wind turbines: a buyers guide. Available at: http://www.ampair.com/sites/all/files/product/resources/PBO%20Magazine.pdf